Gold Nanoparticles as a Vaccine Platform: Influence of Size and Shape on Immunological Responses *in Vitro* and *in Vivo*

Kenichi Niikura,[†,*] Tatsuya Matsunaga,[‡] Tadaki Suzuki,[§] Shintaro Kobayashi,[⊥,∥] Hiroki Yamaguchi,[⊥,∥] Yasuko Orba,[⊥] Akira Kawaguchi,[§] Hideki Hasegawa,[§] Kiichi Kajino,[¶] Takafumi Ninomiya,[#] Kuniharu Ijiro,[†] and Hirofumi Sawa[⊥,∥]

[†]Research Institute for Electronic Science (RIES), Hokkaido University, N21W10, Sapporo 001-0021, Japan, [‡]Graduate School of Chemical Sciences and Engineering, Hokkaido University, Sapporo 060-8628, Japan, [§]Department of Pathology, National Institute of Infectious Diseases, Tokyo 162-8640, Japan, [⊥]Division of Molecular Pathobiology, Research Center for Zoonosis Control, Hokkaido University, Sapporo 001-0020, Japan, [∥]Global COE Program, Hokkaido University, Sapporo 060-0818, Japan, [¶]Division of Collaboration and Education, Research Center for Zoonosis Control, Hokkaido University, Sapporo 001-0020, Japan, and [#]Sapporo Medical University School of Medicine, Sapporo 060-8556, Japan

ABSTRACT This paper demonstrates how the shape and size of gold nanoparticles (AuNPs) affect immunological responses *in vivo* and *in vitro* for the production of antibodies for West Nile virus (WNV). We prepared spherical (20 and 40 nm in diameter), rod (40 × 10 nm), and cubic (40 × 40 × 40 nm) AuNPs as adjuvants and coated them with WNV envelope (E) protein. We measured anti-WNVE antibodies after inoculation of these WNVE-coated AuNPs (AuNP-Es) into mice. The 40 nm spherical AuNP-Es (Sphere40-Es) induced the highest level of WNVE-specific antibodies, while rod AuNP-Es (Rod-Es) induced only 50% of that of Sphere40-E. To examine the mechanisms of the shape-dependent WNVE antibody production, we next measured the efficiency of cellular uptake of AuNP-Es into RAW264.7 macrophage cells and bone-marrow-derived dendritic cells (BMDCs) and the subsequent cytokine secretion from BMDCs. The uptake of Rod-Es into the cells proceeded more efficiently than those of Sphere-Es or cubic WNVE-coated AuNPs (Cube-Es), suggesting that antibody production was not dependent on the uptake efficiency of the different AuNP-Es. Cytokine production from BMDCs treated with the AuNP-Es revealed that only Rod-E-treated cells produced significant levels of interleukin-1β (IL-1β) and interleukin-18 (IL-18), indicating that Rod-Es activated inflammasome-dependent cytokine secretion. Meanwhile, Sphere40-Es and Cube-Es both significantly induced inflammatory cytokine production, including tumor necrosis factor-α (TNF-α), IL-6, IL-12, and granulocyte macrophage colony-stimulating factor (GM-CSF). These results suggested that AuNPs are effective vaccine adjuvants and enhance the immune response *via* different cytokine pathways depending on their sizes and shapes.

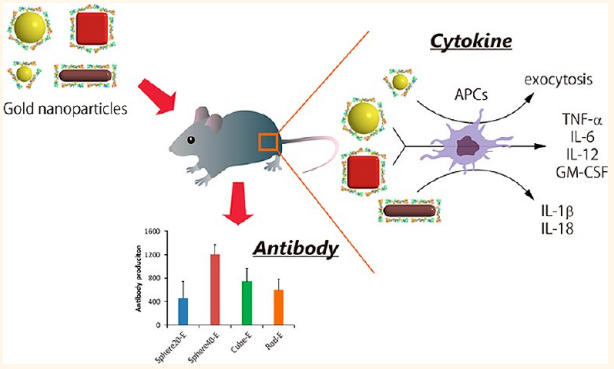

KEYWORDS: gold nanoparticle · vaccine · colloid · west nile virus · cytokine · antibody · shape dependence

Recent efforts to make effective and safe vaccines have focused on the development of subunit vaccines in which an antigen alone is linked to a strong immunogen, such as keyhole limpet hemocyanin (KLH) proteins.[1−3] However, issues remain regarding the use KLH as a vaccine platform. The antigen-KLH conjugate induces antibodies specific for both antigens and KLH, making multiple vaccinations inefficient due to the exclusion by KLH-specific antibodies.[4−6] In order to avoid antibody production against the platform materials, inorganic nanoparticles, in particular, gold, are strong candidates. In fact, gold nanoparticles (AuNPs) have already been used as antigen carriers for subunit vaccines without the production of anti-AuNP antibodies.[6] AuNPs have attracted attention as a nanomaterial in the biomedical

* Address correspondence to kniikura@poly.es.hokudai.ac.jp.

Received for review December 10, 2012 and accepted April 30, 2013.

Published online April 30, 2013
10.1021/nn3057005

© 2013 American Chemical Society

field due to their unique characteristics,[7−11] such as their biocompatibility[10] and easy fabrication in terms of size and shape.[12,13] Tohyama *et al.* first reported the production of antibodies in mice using glutamate-immobilized AuNPs.[14] Subsequently, the usefulness of AuNPs as an antigen carrier has been demonstrated for antigens derived from various viruses including influenza[15] and foot-and-mouth disease.[6,15] In these studies, conventional adjuvants, such as complete Freund's adjuvant or alum, which are used for enhanced induction of immunity, were coadministered with nanoparticle (NP) vaccines.

Recently, there have been a few reports that NPs alone can induce immunological responses, such as antibody and cytokine secretion.[16−18] Antigen-presenting cells (APCs), such as dendritic cells and macrophages, phagocytose external molecules/materials and stimulate lymphocytes and other immune cells by releasing chemical mediators, called cytokines, that initiate an adaptive immune response.[19,20] Hence, an understanding of the effects of nanoparticles on cytokine release is essential for their further application to vaccine adjuvants.[21] Tsai *et al.* reported that the expression levels of cytokines from macrophages after incubation with gold and silver nanoparticles were affected by the nanoparticle diameter.[22] Plebanski *et al.* reported that the size of antigen-immobilized polystyrene beads affected the type-1/type-2 cytokine balance.[17] These data suggest that nanoparticles of a suitable size could provide an effective adjuvant beyond their use as an antigen carrier.

Compared to effect of size, there are few reports on the effect of NP shape on the immunological response. Interestingly, Maysinger *et al.* reported the AuNP shape dependency of the inflammatory response in microglial cells.[23] For instance, the nanourchins increased interleukin-1α production, which is an inflammatory cytokine, but spherical and rod particles did not. These differences in cytokine production in response to nanoparticles of different shapes suggest a desirable alteration in immune response in accordance with changes in the shape of the nanoparticles used.

In this paper, we focused on the NP shape dependency of the immune response *in vivo* as well as *in vitro*. We prepared spherical (20 and 40 nm in diameter), rod (40 × 10 nm), and cubic (40 × 40 × 40 nm) nanoparticles. The nanoparticles were coated with West Nile virus envelope (WNVE) protein to produce 20 and 40 nm spherical (Sphere40-E, Sphere20-E), rod (Rod-E), and cubic (Cube-E) AuNP-Es. West Nile virus (WNV) is distributed over a wide geographical range including North America, Africa, Europe, and the Middle East; however, no practical vaccines for West Nile virus have been developed.[24] We chose these sizes because, in general, for mammalian cells, nanoparticles of 40−60 nm in diameter are known to be well-internalized into cells *via* the endocytotic pathway.[25−27] Further, the size of native WNV is also around 40 nm in diameter.[28] The levels of anti-WNVE antibody production in mice after vaccination with these particles were compared. We found that antibody production is significantly dependent on nanoparticle shape. In order to clarify the shape dependence *in vivo*, the cellular uptake of nanoparticles and subsequent cytokine production using RAW264.7 macrophages and murine bone-marrow-derived dendritic cells (BMDCs) were investigated. The correlations between antibody production, uptake level and cytokine production were discussed in regard to "nanoparticle shape".

RESULTS AND DISCUSSION

Characterization of WNVE-Coated AuNPs (AuNP-Es). Spherical, cubic, and rod AuNPs coated with cetyltrimethylammonium bromide (CTAB) were synthesized *via* a seeding growth method from chloroauric acid as reported previously with slight modifications.[13,29] Spherical AuNPs were synthesized in two sizes (20 and 40 nm in diameter; Figure 1A,B). The prepared AuNPs were then coated by an anionic polymer, poly(4-styrenesulfonic acid-*co*-maleic acid) (PSS-MA),[30] which can electrostatically attach the WNVE in the same orientation[31] as the envelope proteins of the native virus. Importantly, CTAB-originated cytotoxicity was drastically reduced by the PSS-MA coating (data not shown). WNVE, as an antigen, was conjugated with PSS-MA-coated AuNPs *via* an electrostatic interaction, and the resultant AuNP-E complexes were characterized as described below.

The physical characteristics of AuNP-E complexes are shown in Table 1. The shape and size of the synthesized AuNPs were confirmed by scanning transmission electron microscopy (STEM) and UV−vis absorption (Figure 1 and Supporting Information Figures S1 and S2). The diameters of the spherical AuNPs (Sphere20s and Sphere40s) were determined to be 19 ± 1.9 and 43 ± 3.3 nm, respectively (Figure 1A,B). The cubic AuNPs (Cubes) had an edge length of 41 ± 4.8 nm (Figure 1C). The rod AuNPs (Rods) were 36 ± 3.6 nm long and 10 ± 1.2 nm wide (aspect ratio = 3.6, Figure 1D). Surface modifications in each step were confirmed by changes of ζ-potential (Figure 1E). The ζ-potentials for all AuNPs changed from positive to negative (−65 to −22 mV) after PSS-MA coating and were slightly negative (−10 to −24 mV) after WNVE conjugation (Figure 1E). Each AuNP showed the same trend, and Rod showed the highest ζ-potential of −10 ± 0.3 mV.

In order to quantify the number of protein molecules on a single AuNP surface, WNVE molecules attached on the AuNPs were peeled off using sodium dodecyl sulfate (SDS) and the number of protein molecules was estimated by Western blotting (Table 1). The number of immobilized WNVE proteins per particle was 74 ± 4, 52 ± 6, and 46 ± 2 for Sphere40-Es, Cube-Es, and Rod-Es, respectively, so no large differences were observed between these similarly sized (~40 nm)

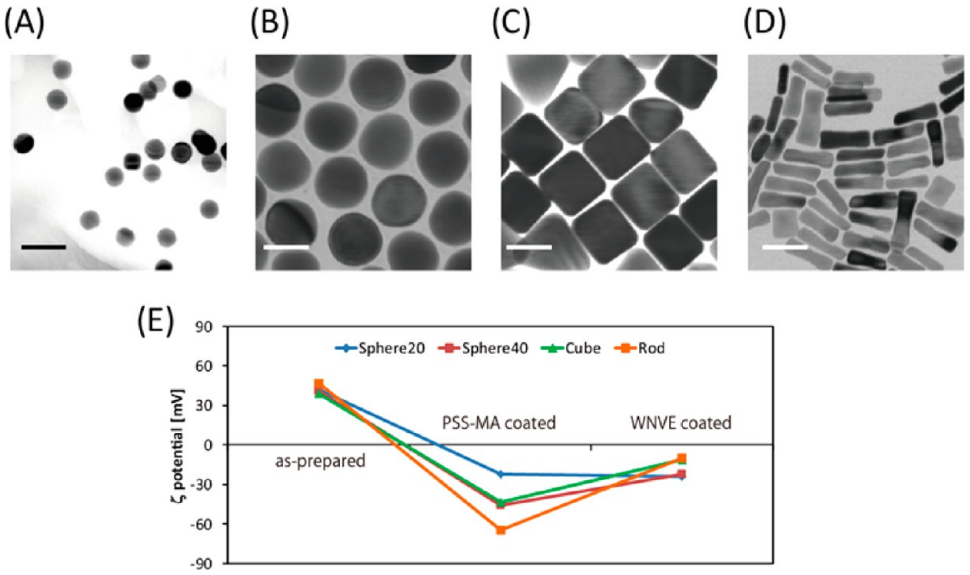

Figure 1. TEM images of as-prepared (A) Sphere20, (B) Sphere40, (C) Cube, and (D) Rod AuNPs. Scale bar represents 40 nm. (E) Zeta-potential (ζ) of AuNPs at each step of surface modification.

TABLE 1. Physical Characteristics of AuNP-E

	diameter (nm)[a]	λ_{max} (nm)	ζ-potential (mV)	number of protein/particle
Sphere20-E	19 ± 1.9	522	−24 ± 3	9.7 ± 3
Sphere40-E	43 ± 3.3	525	−23 ± 1	74 ± 4
Cube-E	41 ± 4.8	539	−11 ± 0.5	52 ± 6
Rod-E	(36 ± 3.6) × (10 ± 1.2)	516, 780	−9.9 ± 0.3	46 ± 2

[a] Determined from TEM images (means ± SD of 200 AuNPs).

particles. For Sphere20-Es, 9.7 ± 3 proteins were immobilized on the surface of a single nanoparticle. Immobilized WNVE molecules were not exchanged with serum protein during incubation for 2 h in a cell growth medium containing 10% fetal bovine serum (FBS) due to the slow exchange reaction rate of WNVE and serum protein (data not shown).

Colloidal Stability of AuNP-Es in a Biological Medium. As the proteins present in biological media interact with nanoparticles and form protein coronas around them,[32,33] shape of nanoparticles could affect protein corona formation so that the colloidal stability of nanoparticles in biological media could be the key feature in the immune response.[34−36] Therefore, the stability of each AuNP-Es in a serum medium (DMEM containing 10% FBS) was examined using dynamic light scattering (DLS) and UV−vis spectrometry (Figure 2). For Sphere40-Es, Sphere20-Es, and Cube-Es, 20−30 nm increases in the hydrodynamic diameter were observed during the initial 6 h of incubation, after which little further change was observed. In contrast, the hydrodynamic diameter, which corresponds to corona formation, was constant for Rod-Es during the initial 6 h period; however, the size suddenly increased after 6 h and reached a size 5 times larger than the original after incubation in serum for 24 h. The aggregation state of nanoparticles can be qualitatively evaluated by red shifts in the plasmon peak. While small shifts (2−6 nm) in the plasmon peak were observed for Sphere40-Es, Sphere20-Es, and Cube-Es during 24 h incubation in serum medium, a large shift (∼20 nm) in the plasmon peak was observed for Rod-Es, supporting the aggregation of Rod-Es indicated by DLS. This means that, for Sphere40-Es, Sphere20-Es, and Cube-Es, incubation in serum induces the formation of a soft corona layer of serum proteins, affording colloidal stability to these AuNP-Es. In contrast, for Rod-Es, incubation in serum for 24 h resulted in only a small aggregation (less than 100 nm) of nanoparticles.

Antibody Responses in Mice Induced by AuNP-E Nanoparticles of Different Sizes and Shapes. The immunogenicity of the AuNP-E nanoparticles was examined in mouse experiments. Groups of 10 mice were intraperitoneally injected twice with 100 ng protein/animal/dose of AuNP-Es, WNVE protein that was not conjugated to AuNPs, or PBS as a negative control. WNVE-specific IgG titers in mice were determined by ELISA using WNVE protein as a coating antigen (Figure 3). The IgG specific to WNVE increased in mice immunized with all of the AuNP-Es. In particular, Sphere40-E showed the highest antibody induction of the four different AuNPs. However, WNVE protein without AuNPs induced almost no anti-WNVE IgG antibodies, similar to the PBS control. These results indicate that AuNPs can enhance antibody induction to the conjugated antigen, suggesting the AuNPs have an adjuvant effect. In addition, the adjuvant effects of AuNPs varied depending on their size and shape. Kojima *et al.* reported that West Nile virus-like particles of two different sizes, 20 and 40 nm, showed different levels of immunogenicity.[37] The larger virus-like particles induced a stronger immunological response than

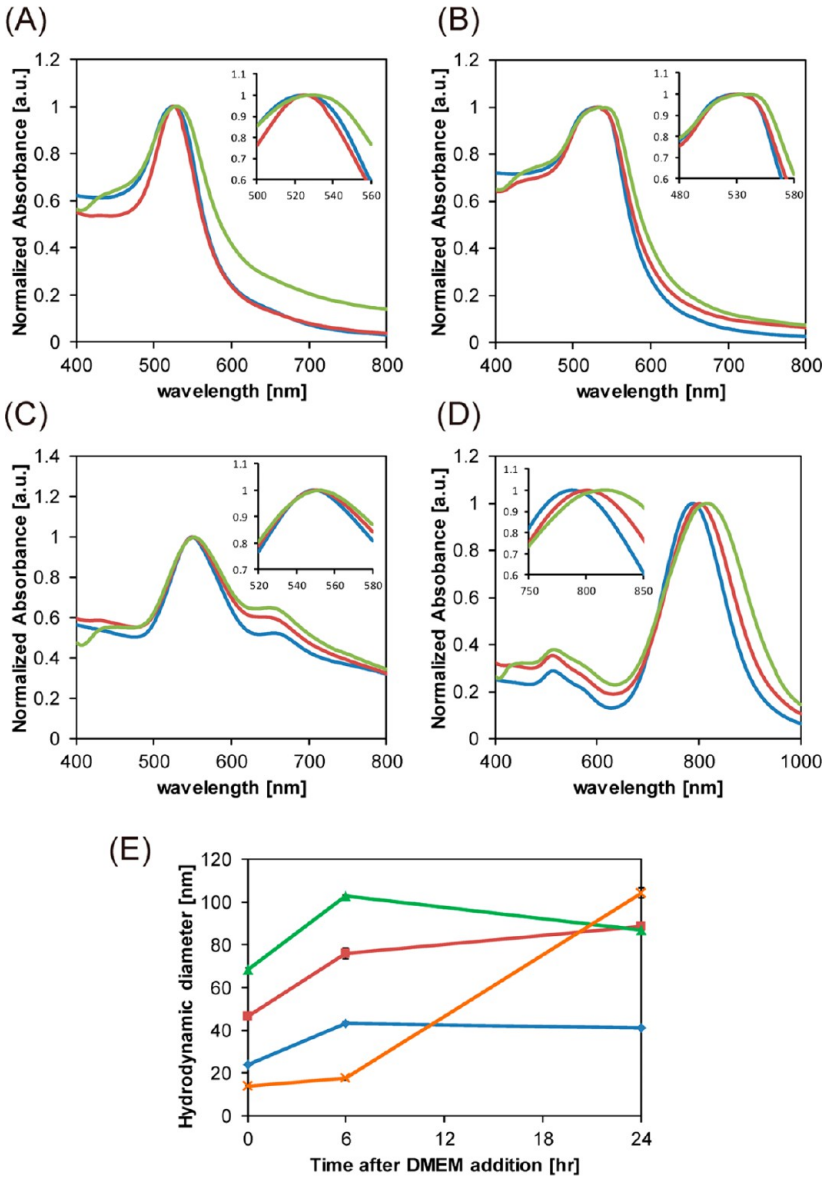

Figure 2. Red shift in absorbance spectra for (A) Sphere20, (B) Sphere40, (C) Cube, and (D) Rod nanoparticles on the addition of cell growth medium containing 10% FBS. Blue, red, and green lines indicate 0, 6, and 24 h after the addition of medium to the AuNP-Es, respectively. (E) Time-course change in hydrodynamic diameters determined by dynamic light scattering (DLS) after the addition of the medium to Sphere20-Es (blue), Sphere40-Es (red), Cube-Es (green), and Rod-Es (orange).

did the smaller ones in the same manner as our results for Sphere40-Es and Sphere20-Es. Notably, there were significant differences in antibody production between spherical, rod, and cubic NPs. The Sphere40-Es induced the highest level of WNVE-specific antibodies, while Rod-Es induced only 50% that of the Sphere40-Es.To explain the shape dependency of antibody production, we carried out *in vitro* studies using APCs based on the following two hypotheses. The first is that differences in the level of uptake of these NPs resulted in differences in the amount of antigen internalized into the APCs. The second is that cytokine production by the APCs is affected by the shape of the nanoparticles.

Comparison of the Cellular Uptakes of Sphere20-E, Sphere40-E, Cube-E, and Rod-E NPs into RAW264.7 Macrophages. At first, we examined the uptake level of the AuNP-Es to validate the first hypothesis using RAW264.7 cells, which are often used as a model for primary macrophages.[38] RAW264.7 cells were incubated with each AuNP-E at a concentration of 5×10^{10} NPs/mL in DMEM. The cytotoxicity of the AuNP-Es was evaluated using a cell-counting kit 8 (CCK-8) assay (Figure S3). None of the AuNP-Es led to obvious cell toxicity compared to the control cells at this concentration. The intracellular distributions of the AuNP-Es after incubation for 1.5 h were observed by confocal laser microscopy (CLMS) (Figure S4). In this experiment, proteins were labeled with Alexa Fluor 647 for their visualization. CLMS data demonstrate that all AuNP-Es were internalized into cells and were distributed outside the nucleus.

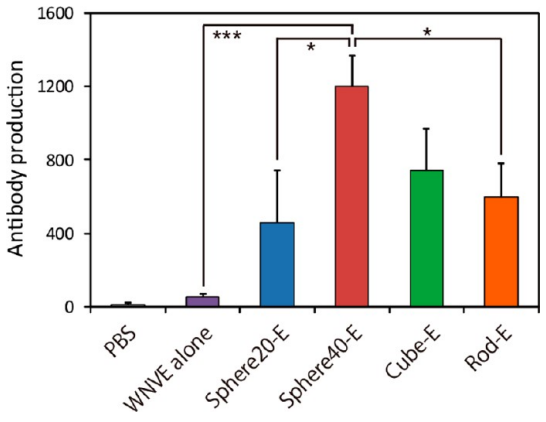

Figure 3. WNVE-specific IgG ELISA end point titers in mice immunized twice at 3 week intervals with 100 ng WNVE/animal/dose of AuNP-E. Antibody production was expressed as the reciprocal of the maximum dilution giving a greater absorbance than sera from PBS-immunized mice. Significant differences: *$p < 0.05$; ***$p < 0.001$ (means ± SEM, $n = 10$).

The level of cellular uptake of the AuNP-Es was detected by inductively coupled plasma atomic emission spectroscopy (ICP-AES) (Figure 4 and Figure S5). ICP-AES data indicate that the number of NPs in a single cell was 25, 7.1, 4.1, and 1.1×10^4 NPs/cell for Rod-Es, Sphere20-Es, Sphere40-Es, and Cube-Es, respectively (Figure 4A). Rod-shaped AuNPs were the most efficiently internalized among the tested particles, with 20% of the total NPs in the medium internalized within 1.5 h. On the contrary, the cubic AuNPs were internalized least efficiently, with only 1.3% of the added NPs entering the cells. The physicochemical properties of NPs, such as surface charge and surface area, are known to influence the cellular uptake of the NPs by macrophages.[39−41] The surface area of rods is similar to that of Sphere20s, and the surface charge of rods is similar to that of cubes. This means that the level of cellular uptake does not simply depend on surface area or charge, rather that shape is another important factor in determining the level of uptake. We also confirmed that AuNPs without a layer of WNVE proteins entered cells in a similar manner to WNVE-coated AuNPs (Figure S5). Frenkel *et al.* reported the effect of the shape of nanoparticles on passive endocytosis using MD simulations and found that the efficiency of endocytosis of spherocylindrical particles (similar in shape to our rods) was higher than that of spherical particles.[42] Ghandehari *et al.* compared the level of cellular uptake of PEGylated rod (10×45 nm) and spherical nanoparticles (50 nm in diameter) by RAW 264.7 macrophages.[41] They reported that the nanorods were taken up to a lesser extent than were the spherical nanoparticles based on the "weight of nanoparticles" in cells. These results seem to be inconsistent with our data. However, as each Sphere40 is 15-fold heavier than each rod, Figure 4A shows that the Sphere40s were more efficiently internalized into cells than rods when compared in terms of the weight of nanoparticles in a single cell. However, it should be noted that the number of internalized rods was 6 times higher than that of Sphere40s, meaning that Rod-Es can deliver WNVE antigens more efficiently into macrophages. Since Sphere40-Es induced the highest level of antibodies, the trend in antibody production shown in Figure 3 cannot be explained by the number of internalized AuNP-Es. This implies that there is another factor beyond the amount of antigen internalized.

Inflammasome Activation: Intracellular Distribution of AuNP-Es in RAW264.7 Cells. Next, we tested the second hypothesis that differences in the shape of the NPs induced differences in the level of cytokine production by APCs. First, we focused on the immunological response *via* inflammasomes, which are cytosolic molecular complexes that activate inflammatory caspase, cytokine IL-1β and IL-18, which promote inflammatory responses.[43,44] Inflammasomes are known to be activated on exposure to nanoparticles due to lysosomal damage, such as the rupture of lysosomes.[45−47] To examine this, the intracellular distribution of AuNP-Es in RAW264.7 cells was visualized by transmission electron microscopy (TEM) and CLMS (Figure S6). Regardless of the size and shape of the AuNPs, TEM images suggested that all AuNPs were taken up *via* the endocytotic pathway (Figure 4B−E). On the one hand, Sphere40-Es and Cube-Es mostly remained in the lysosome (Figure 4C,D), whereas Sphere20-Es and Rod-Es were capable of escaping from the lysosome into the cytosol (Figure 4B,E). CLMS images with lysosome staining by Lysotracker suggested the same trend as that observed in the TEM images (Figure S6). Nevertheless, CLMS images did show some release of Cube-Es from the lysosome, with a small number of Cube-Es also observed to be released in the TEM images (Figure S6E). These results are supported by the MD simulations reported by Frenkel *et al.*, in which small and nonspherical NPs were shown to easily escape from the lipid bilayer.[48] In addition, Sphere20-Es and Rod-Es were removed from cells by exocytosis after culturing for an additional 48 h (Figure 4F). These trends correlate with the lysosomal escape of AuNPs. This lysosomal escape means that Sphere20-Es and Rod-Es have potential cytotoxicity through the rupture of lysosomes and leakage of proteolytic lysosomal enzymes into the cytosol leading to inflammasome activation.

Inflammasome Activation in BMDCs after Exposure to AuNP-Es. IL-1β is a critical pro-inflammatory cytokine involved in the initiation of the innate immune response and regulation of adaptive immunity.[49] The maturation of this cytokine is tightly regulated by the NLRP3 inflammasome.[50] In recent years, there have been a few reports indicating that NPs stimulate NLRP3 inflammasome formation and that the stimulation efficacy depends on the size and surface chemical properties of the NPs.[45,46] Thus, the production of

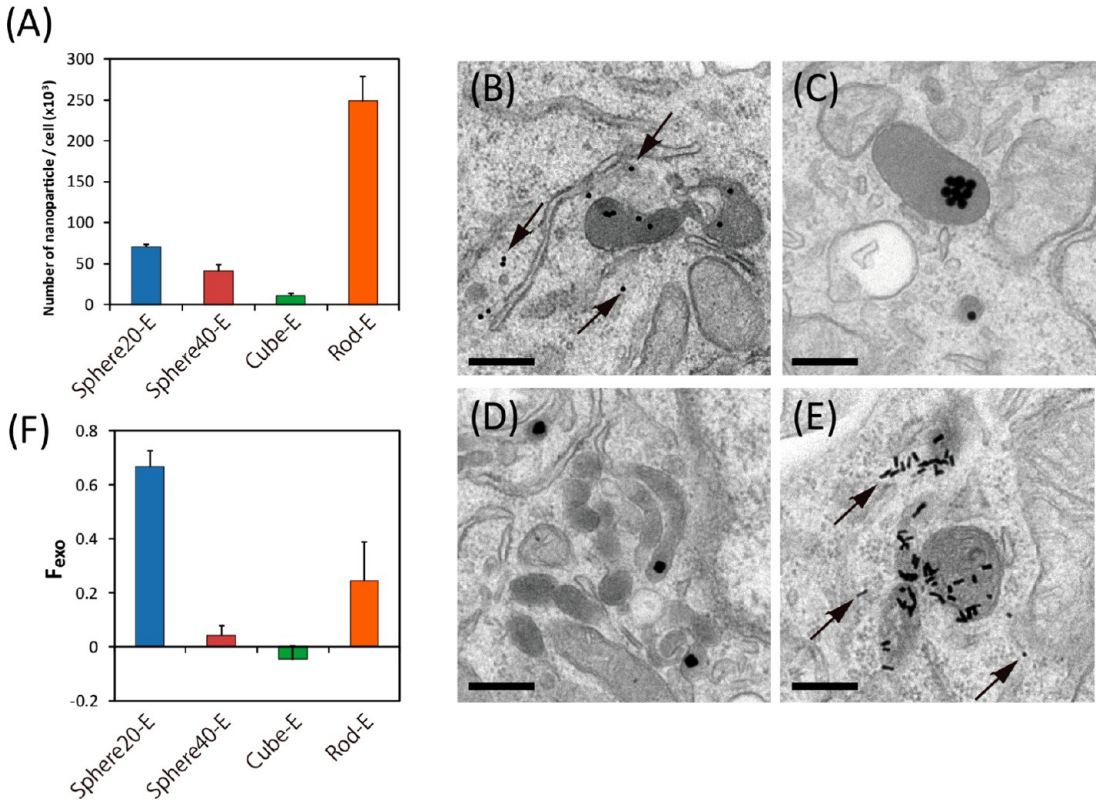

Figure 4. (A) Uptake of AuNP-E by RAW264.7 cells determined from ICP-AES (mean ± SEM, n = 3). TEM images of RAW264.7 cells treated with 2 mg/mL AuNP-Esfor 3 h; (B) Sphere20-E, (C) Sphere40-E, (D) Cube-E, and (E) Rod-E. Arrows indicate AuNP-E in the cytosol. Scale bar represents 300 nm. (F) Exocytotic level of AuNP-Es 48 h after exposure to AuNP-E for 1.5 h. $F_{exo} = N_{out}/N_0$, where N_{out} is the number of NPs exocytosed from the cells and N_0 is the number of NPs internalized before exocytosis (means ± SEM, n = 3).[22]

IL-1β and IL-18 in dendritic cells (DCs) was investigated by ELISA in order to reveal whether the shape-dependent antibody production originated from shape-dependent inflammasome activation or not.

BMDCs were incubated with AuNP-Es at various concentrations, from 2 to 10 μg/mL, for 24 h. CLMS images are shown in Figure 5 (enlarged images in Figure S7). As with RAW264.7 macrophages, AuNP-Es were internalized into cells and distributed outside the nucleus. The black areas within the cells in the DIC images represent internalized AuNP-Es, as the fluorescence from the dye-conjugated AuNP-Es (shown in red in Figure 5) corresponded to these black areas. According to the DIC images, a large number of Rod-Es were taken up, again as seen with RAW264.7 cells. ICP-AES data also supported the significant internalization of rods into the cells (Figure S8).

Cytotoxicity and cytokine production in BMDCs after exposure to AuNP-Es for 24 h in the presence of 50 ng/mL lipopolysaccharide (LPS) is shown in Figure 6. Aluminum potassium sulfate (alum) was used as a positive control for the observation of inflammasome activation.[51,52] LPS increases the amount of pro-IL-1β and pro-IL-18, the immature state of IL-1β and IL-18, in cells.[53] Cytotoxicity occurred in cells treated with Rod-Es at a concentration of 10 μg/mL, although WNVE alone or other AuNP-Es exhibited no cytotoxicity (Figure 6A). IL-1β and IL-18 levels were assessed in the culture supernatants of BMDCs after nanoparticle treatment by ELISA (Figure 6B,C). ELISA results indicated that only Rod-Es evoked IL-1β and IL-18 expression (752 ± 50 and 64 ± 0.8 pg/mL, respectively), while other AuNP-Es or WNVE alone did not. The cytokine production level correlated with the cytotoxicity of Rod-Es. Simmet *et al.* reported that cationic polystyrene nanoparticles induce lysosomal rupture followed by a cytotoxic effect and NLRP3 inflammasome activation.[45] Our rod-shaped AuNPs exhibited lysosomal escape to the cytosol (Figure 4E), and this could be similarly regarded as lysosomal rupture. Although Sphere20-Es can escape from lysosome similarly to Rod-Es, inflammasome activation was not observed. This suggests that the efficiency of internalization of AuNP-Es is one of the important factors to induce the inflammasome-mediated immune response. The cytotoxicity derived from the efficient internalization of Rod-Es and subsequent lysosomal rupture it thought to lead to inflammasome activation with IL-1β and IL-18 secretion. However, this AuNP-E-induced antibody production cannot be fully explained by inflammasome activation as efficient antibody production was also observed for Sphere40-Es and Cube-Es.

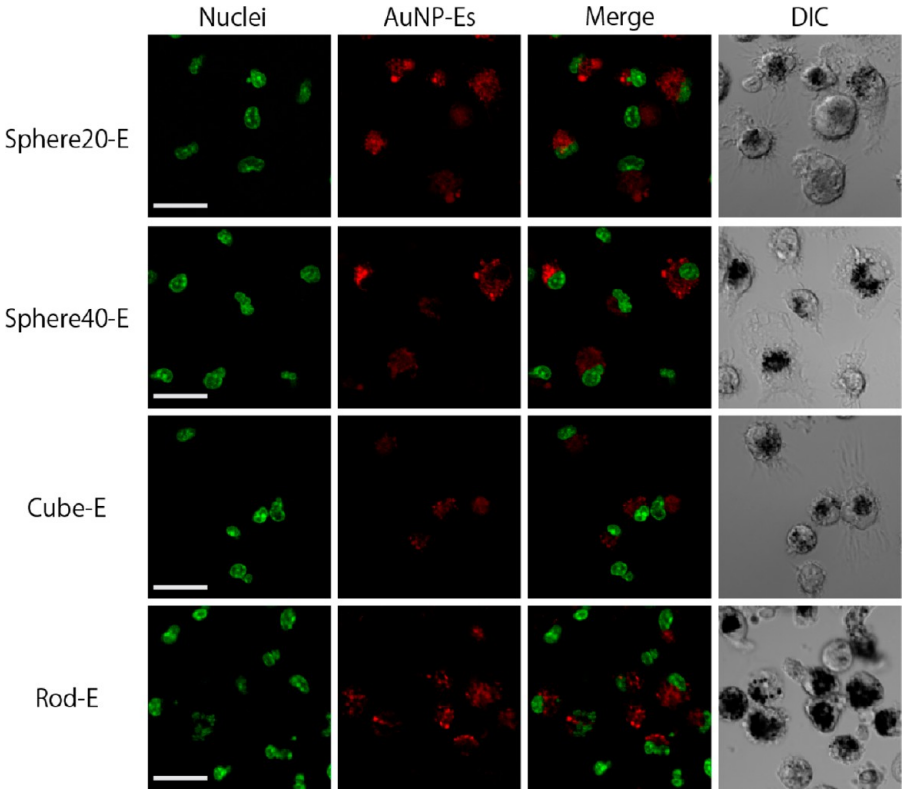

Figure 5. CLMS images of BMDCs treated with 10 μg/mL Alexa Fluor 647-labeled AuNP-Es for 24 h. Nuclei were stained by Hoechst for 30 min (green). Scale bar represents 20 μm.

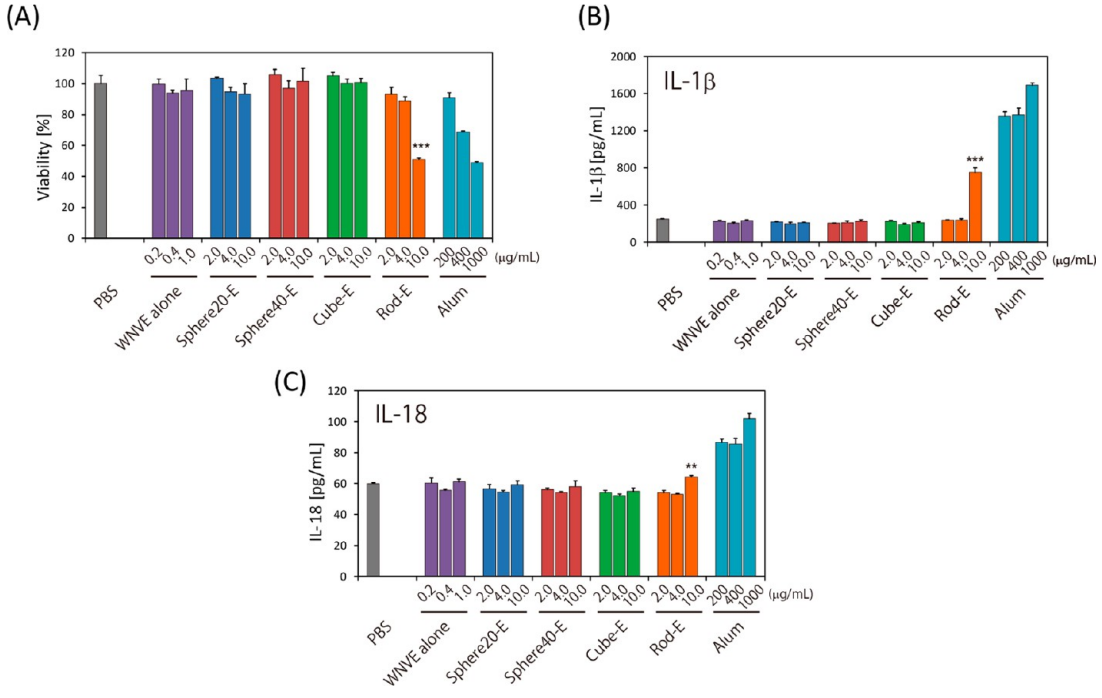

Figure 6. (A) Cytotoxicity of AuNP-Es to BMDCs at various concentrations after incubation for 24 h. (B) IL-1β and (C) IL-18 secretion from BMDCs as an indication of inflammasome activation. Significant differences: **$p < 0.01$; ***$p < 0.001$ *vs* control (means $\pm$ SEM, $n = 3$).

Thus, there is a possibility that APCs recognize the shape of the nanoparticles and induce different cytokines for Sphere40-Es and Cube-Es through non-inflammasome pathway.

Inflammatory Cytokine Secretion from BMDCs after Exposure to AuNP-Es. One of the most important cytokines in the innate and adaptive immune systems is tumor necrosis factor-α (TNF-α), which is a pro-inflammatory cytokine

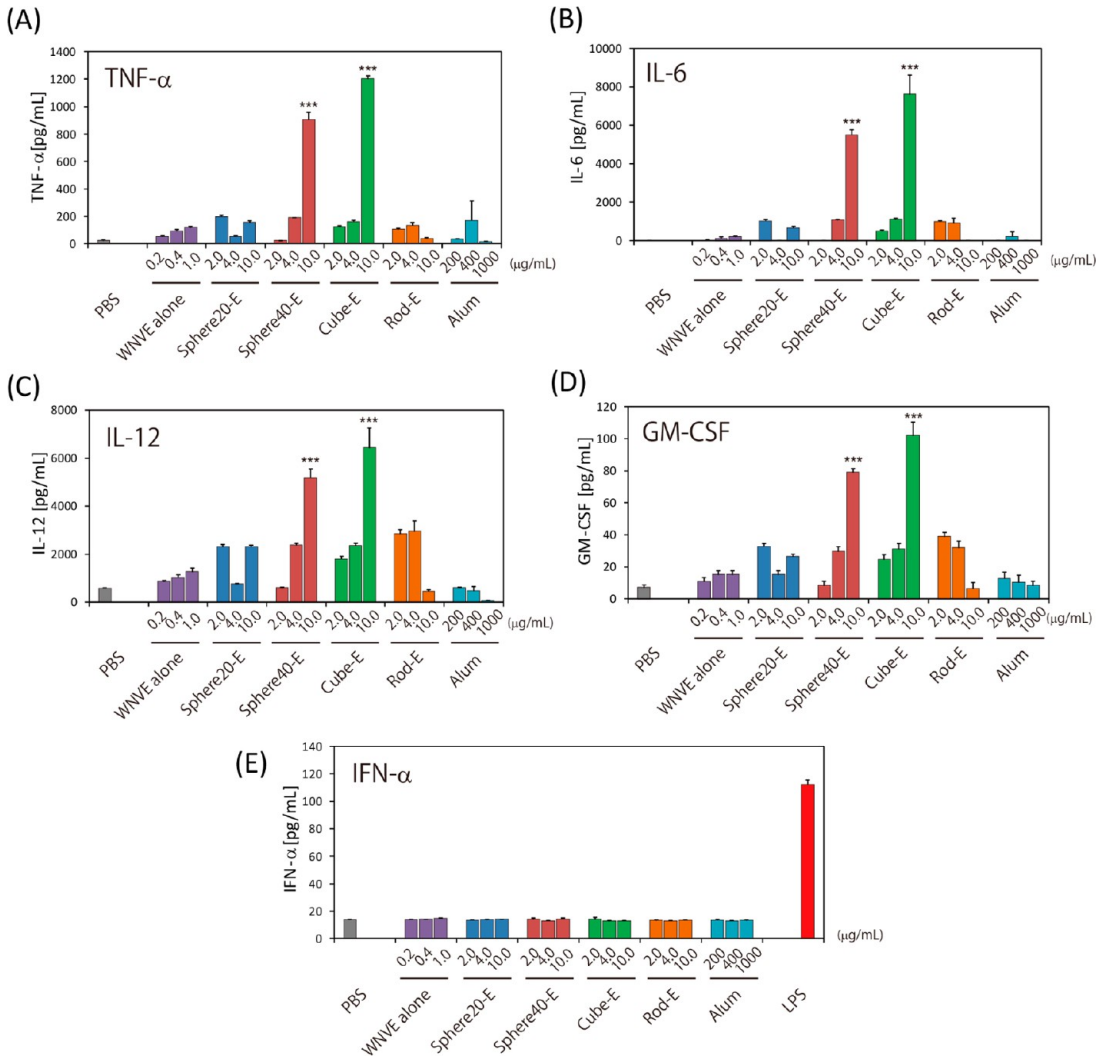

Figure 7. (A) TNF-α, (B) IL-6, (C) IL-12, (D) GM-CSF, and (E) IFN-α secretion from BMDCs treated with AuNP-Es at various concentrations. LPS was used as positive control for IFN-α (50 ng/mL for 3 h, red bar). Significant differences: ***$p < 0.001$ *vs* control (means ± SEM, $n = 3$).

mainly produced by T cells and APCs, such as dendritic cells and macrophages.[54] Importantly, this cytokine is not induced *via* the inflammasome-mediated immune response.[45,55] We examined TNF-α induction from BMDCs after exposure to AuNP-Es (Figure 7A). Sphere40-E and Cube-E NPs induced significantly higher levels of TNF-α (906 ± 50 and 1204 ± 20 pg/mL, respectively) than the other AuNP-Es tested (55−191 pg/mL). We confirmed that the alum adjuvant, which activates the inflammasome-mediated immune response, did not induce TNF-α (16−172 pg/mL). Interestingly, Rod-Es did not induce TNF-α secretion even though the uptake level was markedly higher than those of the other AuNP-Es. Therefore, for the induction of TNF-α, the shape of the AuNP-Es as well as their size is an important factor in the adjuvant function of AuNPs. In addition to TNF-α, induction of other inflammatory cytokines, IL-6, IL-12, and GM-CSF, was also investigated. The induction of IL-6, IL-12, and GM-CSF from BMDCs after treatment with AuNP-Es showed similar trends to that of TNF-α, and only both Sphere40-Es and Cube-Es induced the production of these cytokines (Figure 7B−D). On the contrary, no AuNPs induced interferon-α (IFN-α), which is known to interfere with viral replication in uninfected cells by activating NK cells and macrophages.[56] These data suggest that Sphere40-Es and Cube-Es induce antibodies by the induction of inflammatory cytokines, although these cytokines are different from those induced by Rod-Es. Rod-Es appear to induce antibody production through the inflammasome-mediated pathway (Figure 6). Our *in vitro* experiments clearly demonstrate that AuNP-Es can induce the production of different kinds of cytokines at different levels from dendritic cells in a shape-dependent manner.

Influence of the Physicochemical Parameters of AuNP-Es on Antibody Production and Cytokine Secretion. Although immune responses are also dependent on the pharmacokinetic aspects of the adjuvants *in vivo*, the

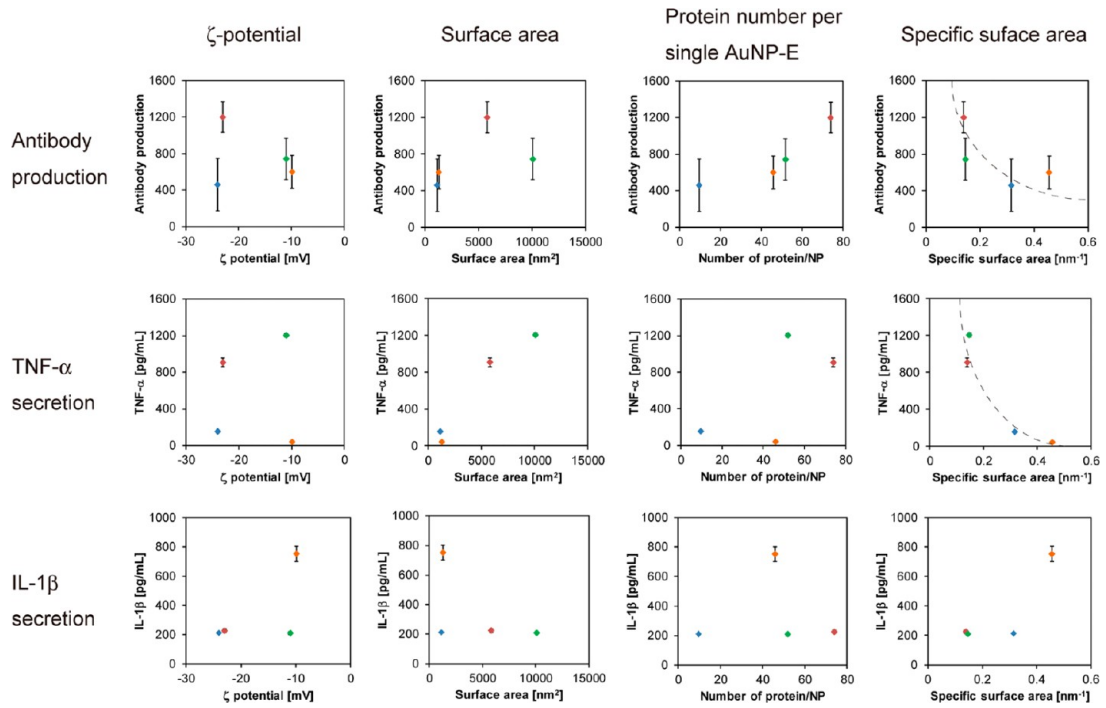

Figure 8. Antibody production or cytokine secretion (TNF-α or IL-1β) *vs* four parameters (ζ-potential, surface area, protein number per single AuNP-E, and specific surface area). Blue, Sphere20-E; red, Sphere40-E; green, Cube-E; orange, Rod-E.

extraction of one specific parameter that dominates immune responses appears difficult. However, we choose four representative parameters for each AuNP-E (surface charge, surface area, protein number per single AuNP-E, and specific surface area, which is the total surface area per single nanoparticle volume (Table S1)) and investigated the correlation between these parameters and antibody production and cytokine secretion (TNF-α or IL-1β) (Figure 8). We note that the specific surface area has an inversely proportional relationship to both antibody production and cytokine secretion. The AuNP-Es with a low specific surface area, such as those with large spherical structures, induced high levels of antibodies and cytokines. In contrast, different effects on antibody and cytokine production were observed for the other parameters. It is known that the size of the spherical nanoparticle presenting the antigen[17] as well as the density of the antigen on the nanoparticle surface[9] is important in producing a strong immune response. On the basis of the above correlations, we propose that specific surface area, which is dependent on both the size and shape of the nanoparticles, is the key factor to simultaneously explain the immune responses observed *in vivo* and *in vitro* in our study. The larger antibody response of Rod-Es compared to that of Sphere20-Es can be explained by the effects of aggregation and their ability to induce high levels of inflammasome-related cytokine secretion. Although the size of nanoparticles has been reported to affect their pharmacokinetics[57−60] and immune responses,[17,22,61] our *in vivo* findings regarding the dependency of immune response on the specific surface area, which is a factor influenced by both size and shape, will be an important factor in the further development of nanoparticle-based vaccines.

CONCLUSIONS

We investigated the effects of shape and size (Sphere40, Sphere20, cube, and rod) of WNVE-coated AuNPs on antibody production in mice. Sphere40 was more effective as a platform than the other shapes (cube and rod) or the smaller sphere (20 nm). For *in vitro* studies using APCs (macrophage and dendritic cells), the rods were most efficiently internalized into these cells and induced the secretion of the inflammasome-related cytokines, IL-1β and IL-18. On the other hand, Sphere40 and cube AuNPs were inefficient for cellular uptake from APCs in comparison to the rods; however, both Sphere40 and cube AuNPs induced the secretion of the pro-inflammatory cytokines, TNF-α, IL-6, IL-12, and GM-CSF, at high levels. We speculated that Sphere40 could efficiently induce antibody production by activating these inflammatory cytokines, whereas rods act *via* inflammasome activation. We note that the specific surface area of AuNPs of various sizes and shapes is a common factor that is correlated to both the secretion of pro-inflammatory cytokines and antibody production. The detailed mechanisms for and generality of the dominant factor underlying the effects of size and shape on immune response, such as aspect ratio, level of protein adsorption, or interaction between nanoparticles and the cell

membrane, should be clarified in a biological environment by further investigation. However, our data for AuNP shape-dependent antibody production and specific cytokine release will contribute to the future design of safe and effective nanoparticle-based vaccines through the activation of the desired immune response.

MATERIALS AND METHODS

Materials. All commercially available reagents were used without further purification. Dulbecco's modified Eagle's medium (DMEM), RPMI-1640, fetal bovine serum (FBS), penicillin, and streptomycin were purchased from GIBCO. The 96-well plates for ELISA were purchased from NUNC (Thermo Fisher Scientific Inc., USA). ECL Western Blotting detection reagents, Precision Plus protein dual color standard, Mini-PROTEAN TGX precast gels, Immun-Blot PVDF membrane and extra thick blot paper were purchased from Bio-Rad Laboratories, Inc. (USA). Mouse anti-WNV envelope IgG and HRP-conjugated anti-mouse IgG were purchased from Abcam plc (UK). IL-1β and TNF-α Quantikine ELISA kits were purchased from R&D Systems, Inc. (USA). IL-18 ELISA kits were purchased from MBL (Japan). Verikine IFN-αELISA kits were purchased from PBL Interferon Source (USA). Other reagents were purchased from Wako Pure Chemical Industries (Japan) and Sigma Aldrich (USA). In all experiments, deionized Millipore water (18 MΩcm^{-1}) was used.

AuNP Synthesis. Gold nanorods (rods) were prepared using a seeding growth method as described previously by Murphy *et al.*[13] Gold nanospheres (20 and 40 nm in a diameter; Sphere20s and Sphere40s, respectively) and nanocubes (cubes) were prepared according to the method reported by Wang *et al.* with modifications,[29] particularly in the case of the nanospheres. Briefly, to a seed solution consisting of $HAuCl_4$ (0.01 M, 250 μL) and CTAB or CTAC (0.1 M, 7.5 mL) was added ice-cold $NaBH_4$ (0.01 M, 600 μL). The resulting seed solution was stirred at room temperature for 2 h. The CTAB-stabilized seeds were used for cube and rod synthesis, and CTAC-stabilized seeds were used for nanosphere synthesis. The growth solution was prepared by the sequential addition of CTAB (0.1 M, 2.9 mL) or CTAB and CTAC (0.1 M, 1.45 mL each), $HAuCl_4$ (0.01 M, 370 μL), and ascorbic acid (0.1 M, 1.8 mL) into water (15 mL). The seed solutions were diluted 10-fold with water. The diluted seed solutions (9.3 μL for Sphere40 and cube, 93 μL for Sphere20) were then added to the growth solution. The resultant solutions were mixed by gentle inversion for 10 s and then left undisturbed overnight at 30 °C.

Scanning transmission electron microscopic (STEM) images were obtained using a STEM HD-2000 system (Hitachi High-Tech Manufacturing & Service Co., Ltd., Japan) with 200 kV accelerating voltage. UV−vis spectra were measured with a UV−vis spectrophotometer (UV-1650PC; Shimadzu Corporation, Japan).

Preparation of West Nile Virus Envelope (WNVE) Protein. Water-soluble His-tagged ectodomain of WNVE protein (NY99 6LP strain) was produced by a persistently expressing 293T cell line. WNVE protein was purified by immobilized metal ion affinity column chromatography with a Ni-NTA column (GE) in accordance with the manufacturer's instructions. The elution fractions were assessed by SDS-PAGE, and those fractions containing WNVE protein were pooled. The purified E protein was then dialyzed overnight at 4 °C against PBS and concentrated using a 30 kDa molecular weight cutoff (MWCO) AmiconUltra filter unit (Millipore).

For cell imaging, the WNVE protein was modified with Alexa Fluor 647 carboxylic acid and succinimidyl ester (Life Technologies) by incubation for 1 h at room temperature.

AuNP−Protein Complex (AuNP-E) Preparation. The synthesized AuNP solutions were purified by centrifugation twice using a CF-16RX system (Hitachi-Koki, Ltd., Japan) to remove excess CTAB (2000−4000*g*, 10 min each). According to previous report published by Murphy *et al.*,[30] a poly(4-styrenesulfonic acid-*co*-maleic acid) sodium salt (PSS-MA; 1:1 4-styrenesulfonic acid/maleic acid mole ratio, MW ~ 20 000 g/mol) solution (10 mg/mL, 200 μL) was added to the AuNP solutions (1 mL), and the resultant mixtures were vortexed for 30 s. After adsorption for 1 h, the excess polymer in the supernatant fraction was removed by centrifugation twice (2000−4000*g*, 10 min each) followed by resuspension in water. WNVE protein (10 μg) was added to the polymer-coated AuNP solutions, and the mixtures were incubated at 30 °C for 1 h. After adsorption, the excess protein in the supernatant fraction was removed by centrifugation twice (2000−4000*g*, 10 min each) followed by resuspension in PBS.

Quantification of WNVE Protein on AuNPs. The AuNP-E solutions were concentrated by centrifugation and then added to SDS-PAGE sample buffer to peel off proteins from the surface of the AuNPs. After heating at 95 °C for 5 min for denaturation of the proteins, the solutions were centrifuged (6000*g*, 5 min) to completely precipitate the AuNPs. The supernatants were applied to SDS-PAGE with WNVE protein of known concentrations and then transferred to a PVDF membrane using a semidry method. The transferred membrane was analyzed by Western blotting with mouse anti-WNV envelope IgG and HRP-conjugated anti-mouse IgG. Immunoreactive proteins were detected with ECL detection reagent and quantified by densitometry using a LAS-3000 imaging system (FUJIFILM, Japan).

Absorbance and Dynamic Light Scattering (DLS) Measurement in Biological Medium. The AuNP-E solutions were added to DMEM supplemented with 10% fetal bovine serum (FBS) and incubated for 24 h. At 0, 6, and 24 h, absorbance spectra and hydrodynamic diameters were measured using a UV−vis spectrophotometer and Delsa Nano HC (Beckman Coulter, USA).

Immunization and Analysis of Antibody Responses. Groups of ten 4-week-old female C3H/HeNJc1 mice (CLEA Japan, Inc., Japan) were intraperitoneally immunized twice at 3 week intervals with 100 ng protein/animal of AuNP-Es, PBS, or WNVE protein solution. Sera were collected at 1 week after the second immunization. The anti-WNVE immunoglobulin G (IgG) titers of the individual mouse sera were determined using ELISA plates coated with WNVE protein and HRP-conjugated antimouse IgG. Immunoreactive proteins were detected with SIGMAFAST OPD. After reaction, the absorbance at 450 nm was measured. Absorbance cutoff values were calculated as the mean absorbance of sera from PBS-immunized mice. Antibody production was expressed as the reciprocal of the maximum dilution giving an absorbance greater than the cutoff value.

Generation of BMDCs. Bone-marrow-derived dendritic cells (BMDCs) were generated from mouse BM as previously described.[62,63] In brief, BM cells of 6-week-old male C3H/HeNJc1 mice were depleted of T cells, B cells, macrophages, and granulocytes by killing with lineage-specific antibodies and complement. Subsequently, the cells were cultured in RPMI-1640 supplemented with 10% FBS, 10 ng/mL recombinant mouse granulocyte/macrophage colony-stimulating factor (rmGM-CSF; R&D Systems), and 50 μM β-mercaptoethanol for 6 days in 24-well culture plates. The culture medium was changed for fresh medium every 2 days. We usually acquired 4×10^6 immature DCs from each mouse.

Cell Culture and Treatment with AuNP-Es. RAW264.7 cells were maintained in DMEM supplemented with 10% FBS, 500 units/mL penicillin, and 500 μg/mL streptomycin. Cells were seeded at 10^5 cells/well in 6-well cell culture plate or 35 mm glass-bottomed dishes (Asahi Glass Co. Ltd., Japan) and treated 24 h later. In the case of BMDCs, cells were seeded at 10^5 cells/well in triple-well glass-based dishes. The cultures were kept at 37 °C in a humidified incubator under a 5% CO_2 atmosphere.

In cell imaging experiments, AuNP-Es conjugated with Alexa Fluor 647 were added to the cell dishes at a final concentration at 5×10^{10} NPs/mL. After incubation in an incubator for 1.5 h, the cells were washed with PBS three times to remove AuNP-Es that did not enter the cells and then added to fresh culture medium. For colocalization observation of AuNP-Es and lysosomes, 50 nM Lysotracker Blue DND-22 in cell culture medium

was added. After incubation for 30 min, cells were washed with PBS three times and added to fresh medium. These cell samples were then ready for imaging measurements. Fluorescence and differential interference contrast (DIC) images were obtained using a confocal laser scanning microscope (CLMS; Olympus FV-300). The cell imaging experiments were done under same conditions, including laser power and photomultiplier gain, on the same day. In BMDC imaging experiments, BMDCs were treated with 10 μg/mL AuNP-Es for 24 h. After exposure to AuNP-Es, cell culture supernatants were removed and 0.2 μg/mL Hoechst in cell culture medium was added. After incubation for 20 min, cells were washed with PBS three times and added to fresh culture medium.

In cellular uptake and removal experiments, AuNP-Es were added to the cell dishes under the same conditions as in the cell imaging experiments, and washing was performed in the same manner. For the removal experiment, the cells were cultured for a further 48 h and washed three times. The cells were treated with aqua regia, and the cell dispersion was further sonicated for 1 min to completely disrupt the cell membranes and dissolve AuNPs to gold ions. The resultant solutions were diluted with water (6 mL). The concentrations of gold ions in the cells were determined by ICP-AES (ICPE-9000, Shimadzu) after obtaining a calibration curve for the gold ions at various concentrations using commercial standards. The concentrations of gold ions contained in the cells were then converted to the number of gold nanoparticles taken up per cell by consideration of the size of the nanoparticles obtained from the STEM imaging and the total number of cells involved.

TEM Observation. RAW264.7 cells were incubated with the AuNP-Es (final concentration: 2 μg/mL) for 3 h in DMEM on BioCoat poly-D-lysine 8-well CultureSlides (BD). After washing with PBS buffer, the cells were fixed in 2.5% glutaraldehyde/0.1 M phosphate buffer (pH 7.4) overnight at 4 °C, postfixed in a mixed aqueous solution of 1% osmium tetroxide and 1.5% potassium ferrocyanide for 2 h at room temperature, dehydrated in a graded ethanol series, and embedded in Epon 812 (TAAB). Ultrathin sections were then cut on a RMC Ultramicrotome MTX. The sections were stained with uranyl acetate followed by lead citrate and examined at 80 kV with a JEM-1400 transmission electron microscope (JEOL, Japan).

Cytokine Production Measurement. BMDCs were first primed with 50 ng/mL LPS for 3 h. After priming, the cells were seeded at 10^5 cells/well in 96-well cell culture plate. The cells were then treated with 50 ng/mL LPS and AuNP-Es at various concentrations for 24 h. The level of IL-1β and IL-18 was measured by ELISA following the manufacturer's protocols. For several cytokine and chemokine measurements, BMDCs were not primed with LPS. Culture supernatants were collected and tested for cytokine levels by LUMINEX (IL-6, IL-12, and GM-CSF) using the mouse cytokine Ten-Plex antibody bead kit (Invitrogen) or ELISA (TNF-α and INF-α) following the manufacturer's protocols.

Cytotoxity Assay. Cells were seeded at 10^4 cells/well (RAW264.7 cell) or 10^5 cells/well (BMDC) in 96-well cell culture plates. Cell viability was tested using a cell-counting kit 8 (CCK-8, Dojindo, Japan). After incubation for 24 h with AuNPs, the medium was removed, and fresh medium (100 μL) containing 10% CCK-8 reagent was added to each well. The culture plates were incubated at 37 °C and 5% CO_2 for 3 h. After incubation, the absorbance at 450 nm was measured using a microplate reader (Infinite 200 PRO, Tecan).

Statistical Analysis. Statistical analysis was carried out using Student's independent *t* test. A value of $p < 0.05$ was considered to be significant.

Conflict of Interest: The authors declare no competing financial interest.

Acknowledgment. We gratefully acknowledge the Cabinet Office, Government of Japan and the Japan Society for the Promotion of Science (JSPS) for financial support through the FIRST Program, grants from the Ministry of Education, Culture, Sports, Science, and Technology (MEXT) and the Ministry of Health, Labor and Welfare, Japan. A part of this work was conducted at Hokkaido Innovation through Nanotechnology Support (HINTS), supported by "Nanotechnology Network JAPAN" Program and the Japan Initiative for Global Research Network on Infectious Diseases (J-GRID), MEXT Japan.

Supporting Information Available: Figure S1–S7 and Table S1 as described in the text. This material is available free of charge *via* the Internet at http://pubs.acs.org.

REFERENCES AND NOTES

1. Harris, J. R.; Markl, J. Keyhole Limpet Hemocyanin (KLH): A Biomedical Review. *Micron* **1999**, *30*, 597–623.
2. Ragupathi, G.; Meyers, M.; Adluri, S.; Howard, L.; Musselli, C.; Livingston, P. O. Induction of Antibodies against GD3 Ganglioside in Melanoma Patients by Vaccination with GD3-Lactone-KLH Conjugate Plus Immunological Adjuvant QS-21. *Int. J. Cancer* **2000**, *85*, 659–666.
3. Hou, Y.; Gu, X. X. Development of Peptide Mimotopes of Lipooligosaccharide from Nontypeable *Haemophilus influenza* as Vaccine Candidates. *J. Immunol.* **2003**, *170*, 4373–4379.
4. May, R. J.; Beenhouwer, D. O.; Scharff, M. D. Antibodies to Keyhole Limpet Homecyanin Cross-React with an Epitope on the Polysaccharide Capsule of *Cryptococcus neoformans* and Other Carbohydrates: Implications for Vaccine Development. *J. Immunol.* **2003**, *171*, 4905–4912.
5. Gharavi, A. E.; Pierangeli, S. S.; Stanfield, M. C.; Liu, X. W.; Espinola, R. G.; Harris, E. N. GDKV-Induced Antiphospholipid Antibodies Enhance Thrombosis and Activate Endothelial Cells *in Vivo* and *in Vitro*. *J. Immunol.* **1999**, *163*, 2922–2927.
6. Chen, Y. S.; Hung, Y. C.; Lin, W. H.; Huang, G. S. Assessment of Gold Nanoparticles as a Size-Dependent Vaccine Carrier for Enhancing the Antibody Response against Synthetic Foot-and-Mouth Disease Virus Peptide. *Nanotechnology* **2010**, *21*, 195101–1951018.
7. Rana, S.; Bajaj, A.; Mout, R.; Rotello, V. M. Monolayer Coated Gold Nanoparticles for Delivery Applications. *Adv. Drug Delivery Rev.* **2012**, *64*, 200–216.
8. De, M.; Ghosh, P. S.; Rotello, V. M. Applications of Nanoparticles in Biology. *Adv. Mater.* **2008**, *20*, 4225–4241.
9. Bastús, N. G.; Sánchez-Tilló, E.; Pujals, S.; Farrera, C.; López, C.; Giralt, E.; Celada, A.; Lloberas, J.; Puntes, V. Homogeneous Conjugation of Peptides onto Gold Nanoparticles Enhances Macrophage Response. *ACS Nano* **2009**, *3*, 1335–1344.
10. Shukla, R.; Bansal, V.; Chaudhary, M.; Basu, A.; Bhonde, R. R.; Sastry, M. Biocompatibility of Gold Nanoparticles and Their Endocytotic Fate Inside the Cellular Compartment: A Microscopic Overview. *Langmuir* **2005**, *21*, 10644–10654.
11. Dykman, L.; Khlebtsov, N. Gold Nanoparticles in Biomedical Applications: Recent Advances and Perspectives. *Chem. Soc. Rev.* **2013**, *41*, 2256–2282.
12. Perrault, S. D.; Chan, W. C. W. Synthesis and Surface Modification of Highly Monodispersed, Spherical Gold Nanoparticles of 50–200 nm. *J. Am. Chem. Soc.* **2009**, *131*, 17042–17043.
13. Sau, T. K.; Murphy, C. J. Room Temperature, High-Yield Synthesis of Multiple Shapes of Gold Nanoparticles in Aqueous Solution. *J. Am. Chem. Soc.* **2004**, *126*, 8648–8649.
14. Shiosaka, S.; Kiyami, H.; Wanaka, A.; Tohyama, M. A New Method for Producing a Specific and High Titre Antibody against Glutamate Using Colloidal Gold as a Carrier. *Brain Res.* **1986**, *382*, 399–403.
15. Chen, Y. S.; Hung, Y. C.; Liau, I.; Huang, G. S. Assessment of the *In Vivo* Toxicity of Gold Nanoparticles. *Nanoscale Res. Lett.* **2009**, *4*, 858–864.
16. Jiang, W.; Kim, B. Y. S.; Rutka, J. T.; Chan, W. C. W. Nanoparticle-Mediated Cellular Response Is Size-Dependent. *Nat. Nanotechnol.* **2008**, *3*, 145–150.
17. Mottram, P. L.; Leong, D.; Irwin, B. C.; Gloster, S.; Xiang, S. D.; Meanger, J.; Ghildyal, R.; Vardaxis, N.; Plebanski, M. Type 1 and 2 Immunity Following Vaccination Is Influenced by Nanoparticle Size: Formulation of a Model Vaccine for

Respiratory Syncytial Virus. *Mol. Pharmaceutics* **2007**, *4*, 73–84.
18. Wang, Y. T.; Lu, X. M.; Zhu, F.; Huang, P.; Yu, Y.; Zeng, L.; Long, Z. Y.; Wu, Y. M. The Use of a Gold Nanoparticle-Based Adjuvant To Improve the Therapeutic Efficacy of hNgR-Fc Protein Immunization in Spinal Cord-Injured Rats. *Biomaterials* **2011**, *32*, 7988–7998.
19. Banchereau, J.; Briere, F.; Caux, C.; Davoust, J.; Lebecque, S.; Liu, Y. J.; Pulendran, B.; Palucka, K. Immunobiology of Dendritic Cells. *Annu. Rev. Immunol.* **2000**, *18*, 767–811.
20. Janeway, C. A., Jr.; Medzhitov, R. Innate Immune Recognition. *Annu. Rev. Immunol.* **2002**, *20*, 197–216.
21. Hubbell, J. A.; Thomas, S. N.; Swartz, M. A. Materials Engineering for Immunomodulation. *Nature* **2009**, *462*, 449–460.
22. Yen, H. J.; Hsu, S. H.; Tsai, C. L. Cytotoxicity and Immunological Response of Gold and Silver Nanoparticles of Different Sizes. *Small* **2009**, *5*, 1553–1561.
23. Hutter, E.; Boridy, S.; Labrecque, S.; Hebert, M. L.; Kriz, J.; Winnik, F. M.; Maysinger, D. Microglial Response to Gold Nanoparticles. *ACS Nano* **2010**, *4*, 2595–2606.
24. Dauphin, G.; Zientara, S. West Nile Virus: Recent Trends in Diagnosis and Vaccine Development. *Vaccine* **2007**, *25*, 5563–5576.
25. Chithrani, B. D.; Chan, W. C. W. Elucidating the Mechanism of Cellular Uptake and Removal of Protein-Coated Gold Nanoparticles of Different Sizes and Shapes. *Nano Lett.* **2007**, *7*, 1542–1550.
26. Fifis, T.; Gamvrellis, A.; Irwin, B. C.; Pietersz, G. A.; Li, J.; Mottram, P. L.; Mckenzie, I. F. C.; Plebanski, M. Size-Dependent Immunogenicity: Therapeutic and Protective Properties of Nano-Vaccines against Tumors. *J. Immunol.* **2004**, *173*, 3148–3154.
27. Chithrani, B. D.; Ghazani, A. A.; Chan, W. C. W. Determining the Size and Shape Dependence of Gold Nanoparticle Uptake into Mammalian Cells. *Nano Lett.* **2006**, *6*, 662–668.
28. Mukhopadhyay, S.; Kim, B. S.; Chipman, P. R.; Rossmann, M. G.; Kuhn, R. J. Structure of West Nile Virus. *Science* **2003**, *302*, 248.
29. Chen, H.; Kou, X.; Yang, Z.; Ni, W.; Wang, J. Shape- and Size-Dependent Refractive Index Sensitivity of Gold Nanoparticles. *Langmuir* **2008**, *24*, 5233–5237.
30. Gole, A.; Murphy, C. J. Azide-Derivatized Gold Nanorods: Functional Materials for "Click" Chemistry. *Langmuir* **2008**, *24*, 266–272.
31. Kanai, R.; Kar, K.; Anthony, K.; Gould, L. H.; Ledizet, M.; Fikrig, E.; Marasco, W. A.; Koski, R. A.; Modis, Y. Crystal Structure of West Nile Virus Envelope Glycoprotein Reveals Viral Surface Epitopes. *J. Virol.* **2006**, *80*, 11000–11008.
32. Walkey, C. D.; Chan, W. C. W. Understanding and Controlling the Interaction of Nanomaterials with Proteins in a Physiological Environment. *Chem. Soc. Rev.* **2012**, *41*, 2780–2799.
33. Casal, E.; Pfaller, T.; Duschl, A.; Oostingh, G. J.; Puntes, V. Time Evolution of the Nanoparticle Protein Corona. *ACS Nano* **2010**, *4*, 3623–3632.
34. Monopoli, M.; Åberg, C.; Salvati, A.; Dawson, K. A. Biomolecular Coronas Provide the Biological Identity of Nanosized Materials. *Nat. Nanotechnol.* **2012**, *7*, 779–786.
35. Maiorano, G.; Sabella, S.; Sorce, B.; Brunetti, V.; Malvindi, M. A.; Cingolani, R.; Pompa, P. P. Effects of Cell Culture Media on the Dynamic Formation of Protein–Nanoparticle Complexes and Influence on the Cellular Response. *ACS Nano* **2010**, *4*, 7481–7491.
36. Gil, P. R.; Oberdörster, G.; Elder, A.; Puntes, V.; Parak, W. J. Correlating Physico-Chemical with Toxicological Properties of Nanoparticles: The Present and the Future. *ACS Nano* **2010**, *4*, 5527–5531.
37. Ohatki, N.; Takahashi, H.; Kaneko, K.; Gomi, Y.; Ishikawa, T.; Higashi, Y.; Kurata, T.; Sata, T.; Kojima, A. Immunogenicity and Efficacy of Two Types of West Nile Virus-like Particles Different in Size and Maturation as a Second-Generation Vaccine Candidate. *Vaccine* **2010**, *28*, 6588–6596.
38. Raschke, W. C.; Baird, S.; Ralph, P.; Nakoinz, I. Functional Macrophage Cell Lines Transformed by Abelson Leukemia Virus. *Cell* **1978**, *15*, 261–267.
39. Hauck, T. S.; Ghazani, A. A.; Chan, W. C. W. Assessing the Effect of Surface Chemistry on Gold Nanorod Uptake, Toxicity, and Gene Expression in Mammalian Cells. *Small* **2008**, *4*, 153–159.
40. Walkey, C. D.; Olsen, J. B.; Guo, H.; Emili, A.; Chan, W. C. W. Nanoparticle Size and Surface Chemistry Determine Serum Protein Adsorption and Macrophage Uptake. *J. Am. Chem. Soc.* **2012**, *134*, 2139–2147.
41. Arnida; Janát-Amsbury, M. M.; Ray, A.; Peterson, C. M.; Ghandehari, H. Geometry and Surface Characteristics of Gold Nanoparticles Influence Their Biodistribution and Uptake by Macrophages. *Eur. J. Pharm. Biopharm.* **2011**, *77*, 417–423.
42. Vácha, R.; Martinez-Veracoechaea, F. J.; Frenkel, D. Receptor-Mediated Endocytosis of Nanoparticles of Various Shapes. *Nano Lett.* **2011**, *11*, 5391–5395.
43. Ghiringhelli, F.; Apetoh, L.; Tesniere, A.; Aymeric, L.; Ma, Y.; Ortiz, C.; Vermaelen, K.; Panaretakis, T.; Mignot, G.; Ullrich, E.; *et al.* Activation of the NLRP3 Inflammasome in Dendritic Cells Induces IL-1β-Dependent Adaptive Immunity against Tumors. *Nat. Med.* **2009**, *15*, 1170–1178.
44. Martinon, F.; Mayor, A.; Tschopp, J. The Inflammasomes: Guardians of the Body. *Annu. Rev. Immunol.* **2009**, *27*, 229–265.
45. Lunov, O.; Syrovets, T.; Loos, C.; Nienhaus, G. U.; Mailänder, V.; Landfester, K.; Rouis, M.; Simmet, T. Amino-Functionalized Polystyrene Nanoparticles Activate the NLRP3 Inflammasome in Human Macrophages. *ACS Nano* **2011**, *5*, 9648–9657.
46. Yang, E. J.; Kim, S.; Kim, J. S.; Choi, I. H. Inflammasome Formation and IL-1β Release by Human Blood Monocytes in Response to Silver Nanoparticles. *Biomaterials* **2012**, *33*, 6858–6867.
47. Hornung, V.; Bauernfeind, F.; Halle, A.; Samstad, E. O.; Kono, H.; Rock, K. L.; Fitzgerald, K. A.; Latz, E. Silica Crystals and Aluminum Salts Activate the NALP3 Inflammasome through Phagosomal Destabilization. *Nat. Immunol.* **2008**, *9*, 847–856.
48. Vácha, R.; Martinez-Veracoechaea, F. J.; Frenkel, D. Intracellular Release of Endocytosed Nanoparticles upon a Change of Ligand–Receptor Interaction. *ACS Nano* **2012**, *6*, 10598–10605.
49. Dinarello, C. A. Biologic Basis for Interleukin-1 in Disease. *Blood* **1996**, *87*, 2095–2147.
50. Zhou, R.; Yazdi, A. S.; Menu, P.; Tschopp, J. A Role for Mitochondria in NLRP3 Inflammasome Activation. *Nat. Immunol.* **2011**, *12*, 199–200.
51. Eisenbarth, S. C.; Colegio, O. R.; O'Connor, W., Jr.; Sutterwala, F. S.; Flavell, R. A. Crucial Role for the Nalp3 Inflammasome in the Immunostimulatory Properties of Aluminium Adjuvants. *Nature* **2008**, *453*, 1122–1126.
52. Li, H.; Willingham, S. B.; Ting, J. P. Y.; Re, F. Cutting Edge: Inflammasome Activation by Alum and Alum's Adjuvant Effect are Mediated by NLRP3. *J. Immunol.* **2008**, *181*, 17–21.
53. Wickliffe, K. E.; Leppla, S. H.; Moayeri, M. Anthrax Lethal Toxin-Induced Inflammasome Formation and Caspase-1 Activation Are Late Events Dependent on Ion Fluxes and the Proteasome. *Cell. Microbiol.* **2008**, *10*, 332–343.
54. Wajant, H.; Pfizenmaier, K.; Scheurich, P. Tumor Necrosis Factor Signaling. *Cell Death Di⊠er.* **2003**, *10*, 45–65.
55. Franchi, L.; Núñez, G. The Nlrp3 Inflammasome Is Critical for Aluminiumhydroxide-Mediated IL-1β Secretion but Dispensable for Adjuvant Activity. *Eur. J. Immunol.* **2008**, *38*, 2085–2089.
56. Bon, A. L.; Schiavoni, G.; D'Agostin, G.; Gresser, I.; Belardelli, F.; Tough, D. F. Type I Interferons Potently Enhance Humoral Immunity and Can Promote Isotype Switching by Stimulating Dendritic Cells *in Vivo*. *Immunity* **2001**, *14*, 461–470.
57. Thakor, A. S.; Jokerst, J.; Zavaleta, C.; Massoud, T. F.; Gambhir, S. S. Gold Nanoparticles: A Revival in Precious Metal Administration to Patients. *Nano Lett.* **2011**, *11*, 4029–4036.
58. Alkilany, A. M.; Lohse, S. E.; Murphy, C. J. The Gold Standard: Gold Nanoparticle Libraries To Understand the Nano–Bio Interface. *Acc. Chem. Res.* **2013**, *46*, 650–661.

59. Alkilany, A. M.; Murphy, C. J. Toxicity and Cellular Uptake of Gold Nanoparticles: What We Have Learned So Far? *J. Nanopart. Res.* **2010**, *12*, 2313–2333.
60. Zhou, C.; Long, M.; Qin, Y.; Sun, X.; Zheng, J. Luminescent Gold Nanoparticles with Efficient Renal Clearance. *Angew. Chem., Int. Ed.* **2011**, *50*, 3168–3172.
61. Sharp, F. A.; Ruane, D.; Claass, B.; Creagh, E.; Harris, J.; Malyala, P.; Singh, M.; O'Hagan, D. T.; Pétrilli, V.; Tschopp, J.; *et al.* Uptake of Particulate Vaccine Adjuvants by Dendritic Cells Activates the NALP3 Inflammasome. *Proc. Natl. Acad. Sci. U.S.A.* **2009**, *106*, 870–875.
62. Inaba, K.; Inaba, M.; Romani, N.; Aya, H.; Deguchi, M.; Ikehara, S.; Muramatsu, S.; Steinman, R. M. Generation of Large Numbers of Dendritic Cells from Mouse Bone Marrow Cultures Supplemented with Granulocyte/Macrophage Colony-Stimulating Factor. *J. Exp. Med.* **1992**, *176*, 1693–1702.
63. Kajino, K.; Nakamura, I.; Bamba, H.; Sawai, T.; Ogasawara, K. Involvement of IL-10 in Exhaustion of Myeloid Dendritic Cells and Rescue by CD40 Stimulation. *Immunology* **2007**, *120*, 28–37.